CrystEngComm

View Online
Dynamic Article Links

Cite this: *CrystEngComm*, 2011, **13**, 3021

www.rsc.org/crystengcomm

PAPER

Growth of hierarchical TiO_2 nanostructures on anatase nanofibers and their application in photocatalytic activity†

Xianhui Meng,[a] Dong-Wook Shin,[b] Seong Man Yu,[b] Jae Hun Jung,[a] Hong Ik Kim,[b] Hyun Myuong Lee,[a] Young-Ho Han,[b] Vasant Bhoraskar[ac] and Ji-Beom Yoo*[ab]

Received 24th October 2010, Accepted 14th February 2011
DOI: 10.1039/c0ce00765j

Three-dimensional hierarchical nanostructures of TiO_2, consisting of high density nanorods on nanofibers, were synthesized by the combination of electrospinning, thermal annealing and hydrothermal methods. The morphologies, crystal structures, surface area, band gap and photocatalytic activity of the hierarchical nanostructures were characterized by Raman microscopy, X-ray diffraction, UV-vis spectroscopy, scanning electron microscopy, transmission electron microscopy and surface area analysis. The results revealed that the nanofibers, synthesized by the electrospinning method followed by the thermal annealing, were of anatase phase. Similarly, the TiO_2 nanorods grown on the anatase nanofibers by hydrothermal reaction in Ti-HCl solution were of rutile phase, with tetragonal shape, and had top square facet morphologies. The diameter and the length of these rutile nanorods could be varied over the range, 10 nm to 400 nm, and 20 nm to 1 um, respectively, by changing the parameters of the hydrothermal reaction. The growth mechanisms of these rutile rods are discussed on the basis of (i) surface roughness of the anatase nanofibers, (ii) presence of the twin planes of anatase layer with structure similar to rutile phase and (iii) Cl/Ti ratio in the solution. The estimated band gap energies of the nanofibers and nanorods were close to 3.2 eV and 3.0 eV. The total surface area of the hierarchical nanostructures could reach up to ~20.41 $m^2 g^{-1}$; while, the pure the anatase nanofibers surface area is ~19.79 $m^2 g^{-1}$. For the first time, such TiO_2 hierarchical nanostructures, rutile nanorods on anatase nanofibers, have been synthesized. The photocatalytic activity of the TiO_2 hierarchical nanostructures was found to be superior to that of pure anatase nanofibers.

1. Introduction

A literature survey indicates that the hierarchical meso- and nanostructures of functional materials are being explored with a focus on controllable compositions, sizes, shapes, and morphologies.[1] TiO_2 is believed to be the most promising presently known material because of its superior photoreactivity, non-toxicity, long-term stability, and low price. TiO_2 as a photocatalyst is widely used in water purification, because many organic compounds can be decomposed and mineralized by the oxidation and reduction processes on the TiO_2 surface. Among various oxides, the two phases of TiO_2, anatase with band gap ~3.2 eV, and rutile with band gap ~3.0 eV, have received the most attention, due to their excellent electronic, chemical and optical properties. An integrated structure of these two phases in the form of nanorods and nanofibers is of great importance due to possible applications in different fields.[2] The synthesis of anatase nanofibers using an electrospinning method was reported in 2003 by Xia *et al.*[3] Subsequently, it has opened a new door for producing controlled hierarchical nanostructures. It has been demonstrated that by combining the electrospinning method with a hydrothermal or chemical method, metal,[4] single[5] and multicomponent metal oxides[6] with different morphologies, such as nanoparticles, nanoplates, nanorods and nanowires, can be grown on electrospun anatase nanofibers. However, homogenous hierarchical structures of nanocomposites seem much harder to synthesis than heterogeneous structures. The second nucleation and growth of the same material on a certain area of the first one is a challenge. Using the vapour and condensation technique, hierarchical nanostructures of ZnO, with 6-, 4-, and

[a]*School of Advanced Materials Science & Engineering (BK21), Sungkyunkwan University, Suwon 440-476, Korea*
[b]*SKKU Advanced Institute of Nanotechnology (SAINT), Sungkyunkwan University, Suwon 440-476, Korea. E-mail: jbyoo@skku.edu; Fax: +82-312907410; Tel: +82312907413*
[c]*Department of Physics, University of Pune, Pune, India*

† Electronic supplementary information (ESI) available: (1) HR-TEM image for pure anatase nanofibers, (2) equivalent absorption coefficient (α_{KM}) for pure anatase nanofibers and hierarchical structure. (3) SEM images of the samples for BET measurement and photocatalyst ability. (4) The UV-vis absorbance spectra of photocatalytic degradation of rhdomine-6G solutions after different periods of time over (A) anatase nanofibers and (B) hierarchical TiO_2. See DOI: 10.1039/c0ce00765j

2-fold symmetries have been prepared.[7] Such work on the growth of TiO_2 rutile on anatase nanofibers has not been attempted. Aydil *et al.* and Grimes *et al.* reported epitaxial growth of rutile rods on the fluorine doped tin oxide (SnO_2 : F) (FTO) glass substrate.[8] This was possible mainly because of the structural similarity between the FTO glass structure and the TiO_2 rutile phase. In the present work, rutile TiO_2 nanorods have been grown on anatase TiO_2 nanofibres, by combining electrospinning, thermal annealing, and hydrothermal methods and applied for decolouration of a dye solution. In this manner, unique nanorod–nanofiber hierarchical nanostructures of the two phases of TiO_2, have been incorporated into a homogeneous nanostructure.

2. Experimental

2.1. Chemicals and materials

The chemicals used in this study were high purity titanium(IV) isopropoxide ($Ti[OCH(CH_3)_2]_4$, 97%), poly(vinyl pyrrolidone) (PVP, M_w 1.3 × 10^6), acetic acid (CH_3COOH, 99.7%), rhodamine 6G (R-6G, dye content 99%) and hydrochloric acid. The DI water used in all experiments was filtered through a Millipore E-pure filtration system with resistivity >18 MΩ m.

2.2. Electrospinning and annealing: anatase nanofibers

One-dimensional TiO_2 nanofibers were prepared by an electrospinning method.[3] Initially, 0.4 g PVP and 2 mL acetic acid were mixed with 7 mL ethanol, and then 1 mL titanium(IV) isopropoxide was added. This solution, after being stirred for 1 h, was loaded into the plastic syringe of an electrospinning system. A few soda lime glass substrates (size 25 mm × 25 mm × 1 mm), were kept on the grounded aluminum foil, mounted at a distance of ~15 cm from the tip of the syringe of the system. After applying a dc voltage ~15 kV at the specified terminal of the system, and adjusting the solution discharge rate to ~0.3 mL h^{-1}, the TiO_2 nanofibers were produced. These nanofibers were collected on the soda lime glass substrates for a period of 5 min. In this manner a number of soda lime glass substrates with nanofibers on the top surface could be obtained. To obtain a large amount of the nanofibers for BET and surface area measurements, another experiment was conducted, in which the nanofibers were collected on an aluminium foil for a period of 10 h.

The as-electrospun nanofibers were initially dried under atmospheric conditions for 5 h, later on annealed in three stages in order to get defect less nanofibers. The step annealing process was carried out at different temperatures and residence time, as per the following sequence; (i) 90 °C-0.5 h, (ii) 310 °C-1.5 h, (iii) 450 °C-2 h, at a heating rate ~150 °C h^{-1}.[9] All the soda lime glass substrates containing the TiO_2 anatase nanofibers were grouped in pairs, and in turn each pair was subjected to hydrothermal reaction in a Ti–HCl solution.

2.3. Hydrothermal reaction: rutile nanorods on anatase nanofibers

A solution, made by mixing 20 mL hydrochloric acid with 20 mL water, was kept in a Teflon-lined autoclave (maximum volume 63 mL), and stirred for 10 min. Then, after adding a known amount of titanium isopropoxide in the solution, the solution was stirred for another 10 min. Subsequently, a pair of the glass substrates containing the anatase nanofibers was fully immersed in the solution. These glass plates were supported on the walls of the autoclave, at an angle around 30%, with the nanofiber side facing the bottom side. The autoclave was sealed and put into a preheated oven for a preset residence time. For an understanding of the growth mechanism of the TiO_2 nanorods on the anatase nanofibers, parameters for the hydrothermal reaction, namely residence time, temperature, and the amount of titanium isopropoxide were varied from one set of experiment to another. In each set of experiments, only one parameter was varied and the other two parameters were kept constant. The hydrothermal reactions were therefore carried out at different (i) residence times, 1 h, 2 h, 2.5 h and 3 h, in which the temperature and titanium amount were 150 °C and 0.5 g, respectively, (ii) temperatures, 130 °C, 150 °C and 170 °C, in which residence time and titanium amount were 2.5 h and 0.5 g, respectively, and (iii) titanium amount of 0.3 g, 0.5 g, 0.7 g and 1 g, in which residence time and temperature were 2.5 h and 150 °C, respectively. After completion of the hydrothermal residence time, the samples were removed from the autoclave, rinsed with DI water and then dried at room temperature for 12 h.

For BET and surface area measurements, the nanorods were grown on the anatase nanofibers of weight 0.2 g. The solution used was made by mixing 20 mL DI water, 20 mL HCl, and 1 g of titanium isopropoxide. The hydrothermal reaction was carried out for 3 h at 150 °C. After centrifuging and drying at 400 °C for 1 h, three dimensional TiO_2 nanorods in the form of white powder, of weight 0.4 g, could be obtained.

2.4. Characterization

2.4.1. SEM, TEM, XRD and Raman measurements. Scanning electron microscopy (SEM) images of the TiO_2 nanofibers and hierarchical nanostructures at different stages of the experiment were recorded using a JEOL JSM 6700F field emission scanning electron microscope operating at 15 kV. A few typical recorded SEM images are shown in Fig. 1–4. For the TEM study, the samples were made by removing the nanostructures from the glass substrate by scratching, and then dispersing in ethanol, followed by sonication for 10 min. The ethanol based solution was spread on a few copper grids. The transmission electron microscopy (TEM and HRTEM) images and the corresponding selected area electron diffractions (SAED) were recorded using a JEOL JEM 2100F transmission electron microscope, at an accelerating voltage of 200 kV. A few typical recorded TEM images are shown in Fig. 5.The crystal structures of the TiO_2 nanofibers and hierarchical nanostructures synthesized at different temperatures, were characterized by X-ray powder diffraction (XRD) using a Bruker D8 focus diffractometer with Cu-Kα radiation (λ = 0.15406 nm). The recorded XRD spectra are shown in Fig. 6. The Raman measurements of the TiO_2 nanofibers and hierarchical nanostructures synthesized at different temperatures were also carried out by using a RM1000 In via (Renishaw) spectrometer, over 200–900 cm^{-1} at room temperature. The laser line of 514 nm, at

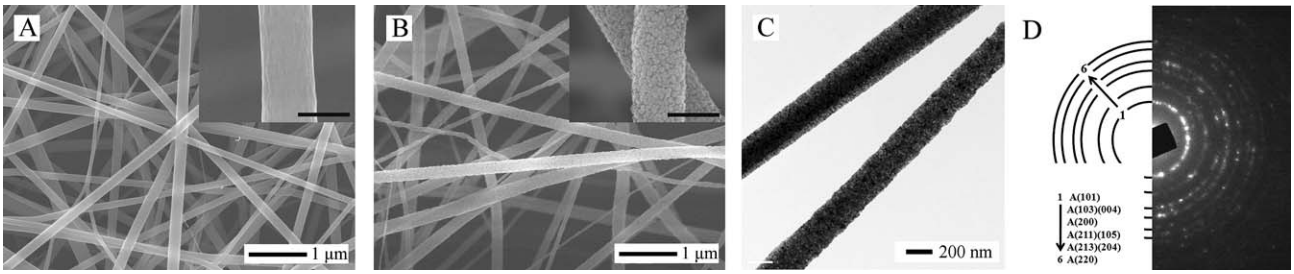

Fig. 1 SEM images of (A) as-electrospun TiO_2/PVP composite nanofibers prepared by the electrospinning method, (B) anatase nanofibers prepared by the optimized calcinations of the TiO_2/PVP composite nanofibers. (C) TEM image of the anatase nanofibers and (D) the corresponding SAED pattern.

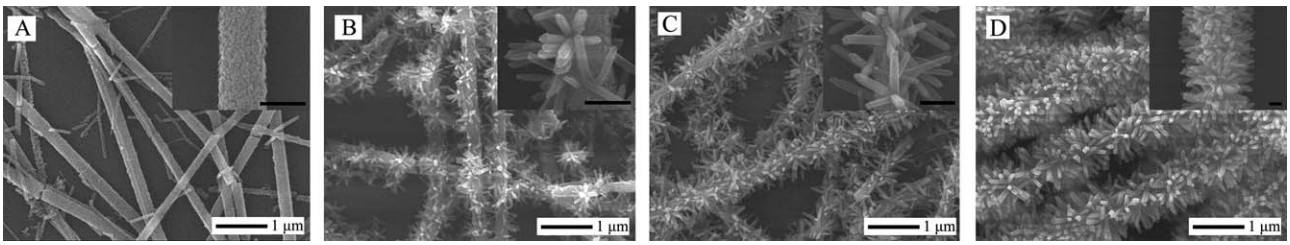

Fig. 2 The SEM images show the evolution of TiO_2 hierarchical structures with the residence times: (A) 1 h, (B) 2 h, (C) 2.5 h and (D) 3 h. For the inset images, the scale bar is 200 nm.

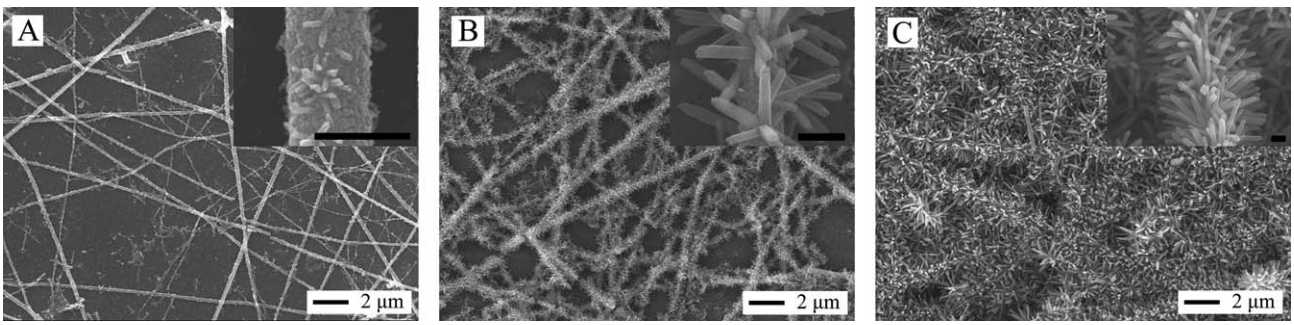

Fig. 3 SEM images of TiO_2 hierarchical nanostructures prepared in a HCl solution containing 0.5 g titanium isopropoxide under hydrothermal reaction for 2.5 h at temperatures of: (A) 130 °C, (B) 150 °C and (C) 170 °C. For the inset images, the scale bar is 200 nm.

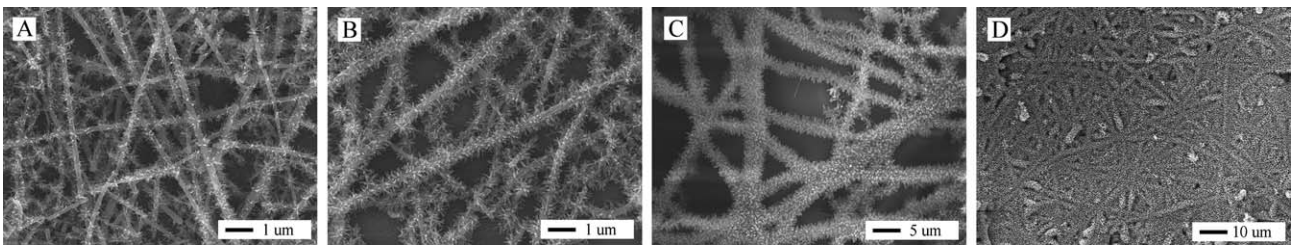

Fig. 4 SEM images of TiO_2 hierarchical nanostructures grown under hydrothermal reaction at 150 °C for 2.5 h in HCl solutions containing different weights of titanium isopropoxide: (A) 0.4 g, (B) 0.5 g, (C) 0.7 g and (D) 1.0 g.

a power level of 20 mW, was used as the excitation source. The recorded Raman spectra are also shown in Fig. 6.

2.4.2. Band gap of the nanofibers and nanostructures. The band gap energies of the nanofibers and TiO_2 hierarchical nanorods prepared using different amounts of titanium isopropoxide were estimated by measuring the diffuse reflectance of the UV-vis spectra, with reference to the reflectance of $BaSO_4$. For this measurement, the anatase nanofibers and the TiO_2 hierarchical nanostructures on the glass substrates in the form of thin films were used. Prior to the measurement, all the thin film samples were thermally treated at 400 °C for 1 h, in order to minimize the effect of crystalline water molecules on the optical measurements. The diffuse reflectance spectra of

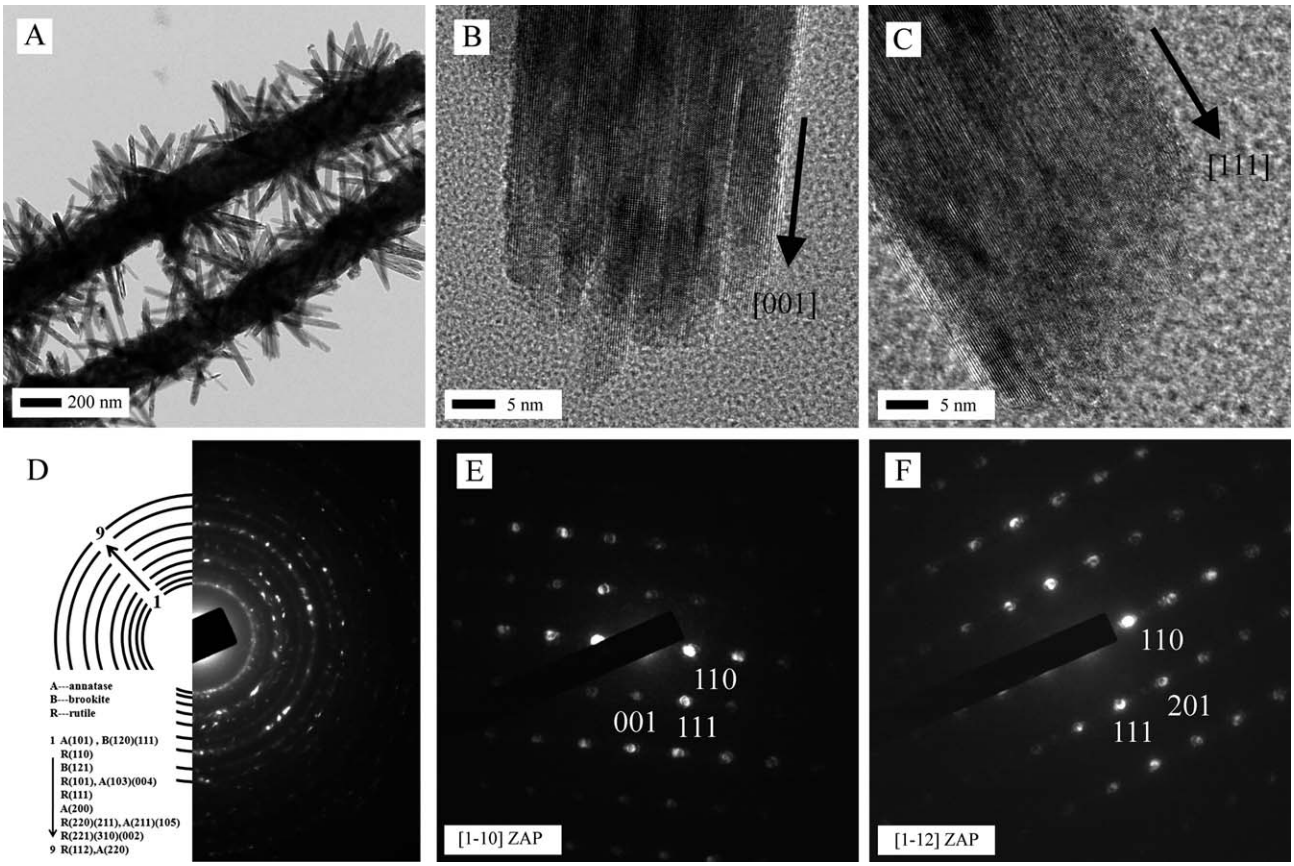

Fig. 5 TEM images of the nanorod–nanofiber hierarchical structures grown in a HCl solution containing 0.5 g titanium isopropoxide under hydrothermal reaction at 150 °C for 2.5 h. (A) image of the recorded hierarchical structures at low magnification and (D) the corresponding responded SAED pattern; (B) HR-TEM image of the top part of a single nanorod, and (E) the corresponding nano beam electron diffraction (NBED) pattern; (C) HR-TEM image of the top part of another single nanorod, and (F) the corresponding NBED pattern.

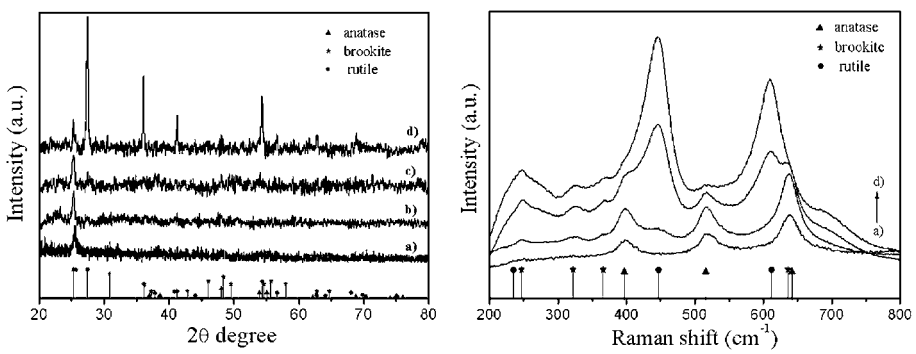

Fig. 6 The recorded XRD spectra and the Raman spectra of the nanorod–nanofiber hierarchical structures. These nanorods were grown in a HCl solution containing 0.5 g titanium isopropoxide under hydrothermal reaction for 2.5 h, at three temperatures. The XRD and Raman spectra correspond to: (a) anatase fiber, (b) 130 °C, (c) 150 °C and (d) 170 °C.

each thin film sample were measured over the wave length range 300–500 nm, using a Shimadzu UV-3600 UV-vis-NIR spectrophotometer.

The results of these measurements for the anatase nanofibers and TiO_2 hierarchical nanostructures are shown in Fig. 7. From the recorded reflectance spectra, the band gap energies of each thin film nanostructures were estimated which are given in the section 3.7.

2.4.3. Surface area measurements. Nitrogen adsorption (BET method) was used for the estimation of the specific surface area of the nanofibers and hierarchical nanostructures. The surface area measurements were performed using a Micromeritics (GeminiIII 2375) surface area analyzer and the surface area was calculated using the standard Brunauer–Emmett–Teller (BET) equation.

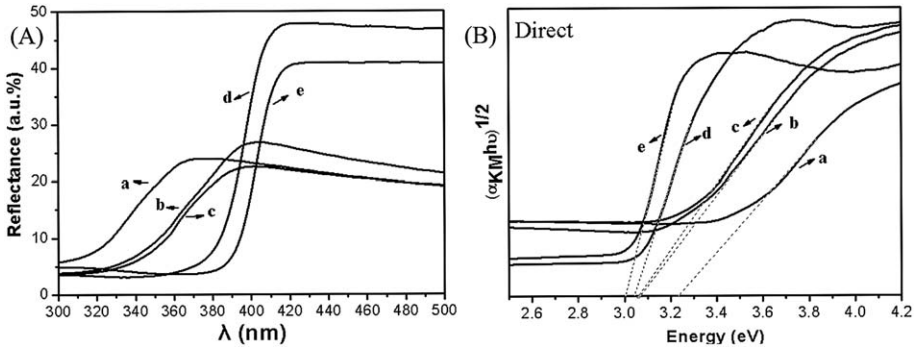

Fig. 7 (A) plots of the UV-vis diffuse reflectance spectra and (B) plots of the band gap energy in direct transition recorded from the anatase nanofibers and nanorod–nanofiber hierarchical structures. The spectrum (a) is anatase nanofibers. The nanorods were grown under hydrothermal reaction at 150 °C for 2.5 h in a HCl solution containing titanium isopropoxide with weights of: (b) 0.4 g, (c) 0.5 g, (d) 0.7 g and (e) 1.0 g.

2.4.4. Photocatalytic activity. The photocatalytic activity of the synthesized anatase nanofibers and the TiO_2 hierarchical nanostructures was separately evaluated on the basis of the decomposition of R-6G in aqueous solution, under exposure of UV radiation. The anatase nanofibers and TiO_2 hierarchical nanostructures, ~0.05 g each, were separately suspended in two different vessels containing ~50 mL 8 ppm concentration R-6G solution. The solutions were stirred in the dark for 30 min to obtain a good dispersion and establish adsorption–desorption equilibrium between the organic molecules and the catalyst surface before irradiation with an intensity discharge 400 μW cm^{-2} UV lamp (365 nm, VL-4.L, Vilber Lourmat, German). At given intervals of illumination (10 min), 7 mL of the reaction solution were taken from both solutions and centrifuged. Subsequently, the absorption spectrum of each solution was measured over 200–700 nm using a Shimadzu UV-3600 UV-vis-NIR spectrophotometer. In the recorded spectrum, the reduction in the absorbance peak at λ ~526 nm was estimated.

3. Results and discussions

3.1. Synthesis of TiO_2 anatase nanofibers

The SEM images in Fig. 1A shows that the one-dimensional TiO_2/PVP composite nanofibers are of different diameters, varying from 200–300 nm with smooth surfaces. The SEM images in Fig. 1B show that the surface roughness of these nanofibers has increased dramatically after calcination as compared to that of as-electrospun TiO_2/PVP composite nanofibers shown in Fig. 1A.This increase in the roughness is attributed to (i) selective removal of the PVP from the nanofibers during the optimized annealing process, and (ii) conversion of the TiO_2/PVP composite nanofibers into polycrystalline anatase TiO_2 phase, as confirmed by the TEM images and SAED pattern shown in Fig. 1C–D.

3.2. Evolution of the TiO_2 nanorods

The SEM images of the TiO_2 nanorods grown on the anatase nanofibers during the different residence time, 1 h, 2 h, 2.5 h and 3 h, respectively, are shown in Fig. 2. It is observed in Fig. 2A that the TiO_2 nanorods did not grow when the residence time was 1 h. Fig. 2B shows that for the residence time of 2 h, the TiO_2 nanorods could grow (i) on the anatase nanofibers covering about 30% of the surface area, (ii) with average length ~150 nm, and diameter varying from 20–30 nm. A detailed analysis of Fig. 2B indicates that a few nanorods are connected to each other in the surface region. Moreover, these nanorods appear nucleated from the same origin, similar to that of the flower-like morphology. However, most of the nanorods are isolated from each other. From the inset image in Fig. 2B, it can be observed that the small TiO_2 nanorods are of tetragonal shape, with top morphologies close to square facets. Fig. 2C shows the SEM image of the nanorods grown for 2.5 h. A detailed analysis reveals that these nanorods have different (i) diameter, varying from 30–40 nm, and (ii) length, varying from 250–300 nm. Moreover, a few large size rods are produced, probably due to agglomeration of small size rods. In Fig. 2D, the SEM image shows that all the nanorods grew for 3 h have almost the same diameter ~100 nm and length ~400 nm. Moreover, the number of the nanorods per unit area increased significantly as a result almost the entire surface of each nanofiber has been decorated with the nanorods. A comparison between the SEM images of Fig. 2 clearly indicates that the length, diameter and density of these nanorods can be increased by increasing the residence time during the hydrothermal reaction.

3.3. Effect of hydrothermal reaction temperature

Fig. 3 shows the SEM images of the TiO_2 nanostructures synthesized in HCl solution containing 0.5 g titanium isopropoxide for 2.5 h under three different temperatures, 130 °C, 150 °C and 170 °C. From Fig. 3A, it can be observed that, at 130 °C, the growth of the nanorods occurred on a very small surface area of the anatase nanofibers. Moreover, these nanorods had an average diameter and length of around 10 nm and 20 nm, respectively. It can be observed in Fig. 3B that at 150 °C, the nanorods could grow on almost 60% of the surface area of the anatase nanofibers, with average length ~250 nm, and diameter ~35 nm. It is interesting to observe in Fig. 3C, that at 170 °C, the nanorods could grow almost on the entire surface area of the anatase nanofibers, with average diameter and length around 110 nm and 900 nm, respectively. Moreover, due to high number density of these nanorods, not a single anatase nanofiber is observed.

3.4. Effect of titanium isopropoxide amount

From the SEM images in Fig. 4A, it is observed that, even at a low concentration of titanium isopropoxide ~0.4 g, the nanorods with an average diameter ~20 nm and length ~100 nm could grow on the anatase nanofibers, however with low number density. Fig. 4B shows that with titanium precursor at ~0.5 g, the nanorods, with an average diameter ~35 nm, and length ~250 nm could grow on almost over 60% of surface area of the anatase nanofibers. It is interesting to observe from Fig. 4C–D that at higher concentration of titanium isopropoxide, both the diameter and the length of the nanorods increased significantly. A detailed analysis of Fig. 4C–D revealed that the average diameter and length of the nanorods were (i) around 100 and 800 nm, respectively, when the weight of titanium isopropoxide was ~0.7 g, and (ii) around 200 nm and 1 μm, respectively, when the weight of titanium isopropoxide was 1.0 g. Moreover, almost the entire surface area of each anatase nanofiber was covered with the nanorods, and therefore, the nanofibers could not be observed in these SEM images. In general, both the density and the size of the nanorods increased with the increase in the amount of titanium isopropoxide.

3.5. Analysis of TEM images

Fig. 5 shows typical TEM images of the nanorod–nanofiber hierarchical structures. It can be observed in Fig. 5A, that the nanostructures exhibit core-shell morphology, with nanorods grown on the surface of the nanofibers. These images further confirm that the entire surface of each TiO_2 nanofiber was covered by the TiO_2 nanorods. The corresponding selected area electron diffraction (SAED) pattern recorded from the same area is shown in Fig. 5D. A detailed analysis of this SAED pattern confirmed that the anatase and rutile phases, along with traces of the brookite phase coexist in these nanostructures. From these nanostructures two nanorods from different locations were selected, and their (i) HR-TEM images are shown in Fig. 5B and 5C, and (ii) the corresponding nano beam electron diffraction (NBED) patterns are shown in Fig. 5E and 5F, respectively. The results indicate that both the rods have single crystal rutile structure, but the growth direction of one of them is [001], while that of the other is [111]. The diameters of a number of nanorods were estimated and found to vary from 30–35 nm. Moreover, it is observed in the TEM images not a single free-standing exists, and therefore these results reveal that the nanorods were heterogeneously nucleated and grew on the surface of anatase nanofibers instead of in the aqueous solution. In the absence of TiO_2 nanofibers, TiO_2 rods could not be synthesized using the same procedure.

3.6. Analysis of the XRD and Raman spectra

In Fig. 6, the recorded XRD spectra in which plot (a) corresponds to the pure nanofibers after annealing. This spectrum has only one peak at 25.35°, which is attributed to the anatase phase of TiO_2 (JCPDS no: 21-1272). The spectra (b) and (c) are of the nanorod–nanofiber hierarchical structures, in which the nanorods were grown under hydrothermal reaction at 130 °C and 150 °C. It is observed that each of the XRD spectra has one prominent peak at 25.35°, which is attributed to the anatase nanofibers. Similarly, the other low intensity peak at 27.44° is attributed to the small rutile phase of TiO_2 nanorods (JCPDS no. 21-1176/88-1172). The XRD spectrum shown in plot (d) is of the hierarchical structures corresponding to 170 °C reaction temperature. In this XRD spectrum, the strong peaks at 27.44°, 36.1°, 41.26°, 54.31° and 62.82° are attributed to (110), (101), (111), (211) and (002) planes of TiO_2 tetragonal rutile phase. The low intensity peak at 30.806 is attributed to the brookite phase of TiO_2 (JCPDS no: 21-1176). This result reveals that the brookite phase of TiO_2 was also formed on the anatase nanofibers, however, at the initial stage of the hydrothermal reaction. As the intensity of the XRD peak increases with the reaction temperature, these results reveal that the size and the number density of the rutile nanorods can also be increased by increasing the reaction temperature.

The Raman spectrum is widely employed in TiO_2 studies, as its three polymorphs belong to different space groups and hence exhibit their characteristic Raman bands.[10] These hierarchical nanostructures prepared at different temperatures were further characterized by the Raman spectrometer, and the results are shown in Fig. 6. The Raman spectrum (a) as shown in Fig. 6 is of the annealed nanofibers made by the electrospinning method. In this Raman spectrum, the peaks at 396 cm^{-1}, 515 cm^{-1}, and 641 cm^{-1} reveal that the annealed nanofibers are of anatase phase. The Raman spectrum (b) is of the nanorods grown on anatase nanofibers at 130 °C. In spectrum (b), the small peaks at 248 cm^{-1}, 324 cm^{-1} and 368 cm^{-1} are attributed to the brookite phase of TiO_2, where the low peaks at 235 cm^{-1} and 447 cm^{-1} are attributed to the rutile phase TiO_2.These results, therefore, further confirm that both brookite and rutile phases of TiO_2 could grow on the anatase nanofibers. In spectra (c) and (d), the prominent peaks at 235 cm^{-1}, 447 cm^{-1} and 612 cm^{-1} correspond to the rutile phase TiO_2. These results of Raman spectroscopy lead to a conclusion that rutile rods have been grown on the anatase nanofibers at different temperatures from 130–170 °C, and support the earlier results obtained from XRD, SEM and TEM measurements

3.7 Band gap measurement

Fig. 7A shows the plots of the diffuse reflectance spectra for the nanofibers and hierarchical nanostructures in the thin film form. These samples were prepared at 150 °C for 2.5 h using different amounts of titanium isopropoxide. In general, for three phase TiO_2 materials, the band gap is 3.00 eV for rutile, 3.13 eV for brookite, and 3.21 eV for anatase, respectively.[11] In the mixture of anatase nanofibers and rutile rods, if the percentage of the rutile rods increases, the reflectance spectra should give a red shift. In Fig. 7A, the red shift into the visible region is clearly observed, with the increase in the coverage of the rutile rods on the anatase nanofibers, as well as the size of the rutile rods. The reflectance spectra were analyzed using the Kubelka–Munk function, $F(r) = (1 - r)^2/(2r)$, to convert the reflectance into the equivalent absorption coefficient (α_{KM}). The details of the analysis are given in Fig. S2 of the ESI.†[12] The direct band gap was estimated from the Tauc plot of the quantity $(F(r)*E)^{1/2}$ against the radiation energy, E, and corresponds to the intercept of the extrapolated linear portion of the plot with the energy axis.[13] Due to the hierarchical nanostructures of the TiO_2 film on

the glass substrate, there may be a small contribution from the light scattering component. However, that contribution should be very small, and therefore may not affect accurate determination of the band gap energy. As shown in Fig. 7B, pure anatase nanofibers show a mean band gap of 3.23 eV, which is close to the literature value. Furthermore, with the growth of the rutile rods, the band gap energy of the hierarchical nanostructures gradually decreased from 3.23 eV to 3.07 eV, 3.06 eV, 3.04 eV and finally reached to 3.00 eV, the band gap energy of the TiO_2 rutile phase.

3.8. Surface area of the nanofibers and hierarchical nanorods

The surface area of nanofibers and hierarchical nanostructures were measured using the BET method. In general, the surface area should be increased as one dimensional nanofibers were modified by one dimensional nanorods, as observed from the SEM images. The value of the measured specific surface area of the TiO_2 nanofiber sample was 19.79 $m^2\ g^{-1}$. Subsequently, the surface area of TiO_2 hierarchical nanostructures synthesized at 150 °C for 2.5 h was found close to 20.41 $m^2\ g^{-1}$. These measurements reveal that after hydrothermal reaction the total surface area of the TiO_2 hierarchical nanostructures was about 2 times higher than that of the pure anatase nanofibers ($0.4 \times 20.41/0.2 \times 19.79$).

3.9 Evaluation of the photocatalytic activity

The photocatalytic activities of the TiO_2 hierarchical nanostructure were evaluated by photocatalytic degradation of R-6G solution. For comparison, the photocatalytic activity of pure anatase nanofibers was also studied under identical conditions. Fig. 8 shows the variation in the concentration of the R-6G in the solution with the period of UV illumination. These photocatalysis results reveal that the hierarchical nanostructures have superior photocatalytic activity as compared to the pure TiO_2 nanofibers. Further observations indicated that the concentration of dye solution changed linearly with increasing illumination time, indicating the complete decomposition of R-6G. The large crystal sizes of the rods did not affect their photocatalytic activity. The enhanced photocatalytic performance of TiO_2 hierarchical nanostructures might be attributed to following factors: (1) better crystallization in single rutile nanorods. A high degree of crystallization is preferred to reduce the formation of electron traps, and therefore, the number of recombination centers of photogenerated electrons and holes reduced to a small value.[14] The crystal faces could also effectively separate the photo genetrated electrons and holes.[15] The 1D exposed single crystal surface of the rutile nanorods allows rapid charge separation between photo-excited electrons and holes and a fast diffusion rate of electrons and holes in the photocatalytic reaction, which can enhance the rate of the photocatalytic reaction. (2) Larger specific surface area. A large specific surface area allows more dye molecules to be absorbed onto the surface of the photocatalyst. The results of the BET analysis revealed that the surface area of the hierarchical nanostructures was greater than that of the nanofibers.

(3) Mixture of two phases of TiO_2 materials. It is widely accepted that the anatase phase of titania is an ideal photocatalytic material among its three crystalline phases.[16] Recently, many groups showed that the photoinduced interfacial electron transfer from anatase to rutile can enhance the photocatalytic activity of TiO_2 materials.[17] When compared with the interface provided by random collisions, a steadier and tighter interface was formed by direct growth of rutile rods on anatase nanofibers which will lead to easier charge transfer and more efficient separation of electron hole pairs before recombination. (4) Higher concentration of acidic surface sites. The surface acidic sites can also enhance the efficiency on the absorption stages.[18] As the rutile nanorods were prepared in acid solution, it is likely that a number of acidic sites might have exited after hydrothermal reaction, even after drying at room temperature. Considering the above factors, it is reasonable to consider that the TiO_2 hierarchical nanostructures prepared by electrospinning and hydrothermal technique can exhibit a photocatalytic activity superior to that of pure TiO_2 nanofibers. Besides this, compared with nanosized TiO_2 powder photocatalyst, such as P25, the TiO_2 hierarchical photocatalyst can be readily separated from the water in a slurry system after photocatalytic reaction because their lengths are at a scale of several micrometres. Therefore, the synthesized TiO_2 hierarchical photocatalyst can be used suitably for the industrial applications. The results indicate that the photocatalytic activity could be further improved by optimization the size, exposed density and the crystal surfaces of the rutile nanorods, in additional to the ratio between anatase nanofibers and rutile nanorods. Further experiments are in process.

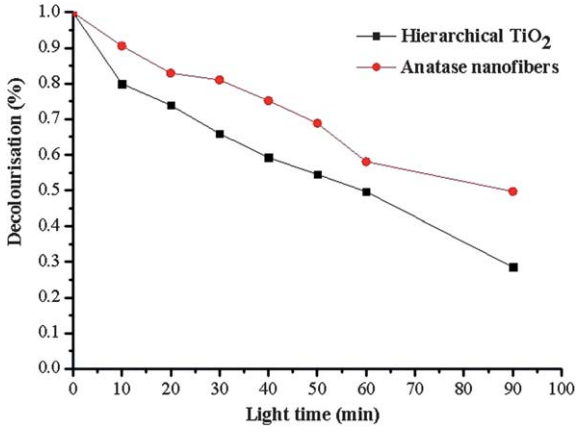

Fig. 8 The plots of the photocatalytic degradation of R-6G in the two separate solutions containing (a) nanofibers and (b) TiO_2 hierarchical nanostructures, under different intervals of UV light illumination.

3.10. Growth mechanism

The mechanism for the observed growth of rutile rods on the anatase nanofibers can be explained by the results of the present study as follows similar to our former research result:[19]

(1) The SEM images show that the anatase nanofibers have rough surface. It has been reported that presence of the indentions, edges, protrusions, *etc.* on the surface can lead to a reduction in the energy barrier for heterogeneous nucleation of nanostructures of metals and semiconductors.[6,7] In addition, heterogeneous nucleation is favoured compared to homogeneous nucleation. In the present work, the rutile rods with different size

and number density have grown preferentially on the rough surface of anatase nanofibers rather than in the solution.

(2) In the hydrothermal reaction, the kinetics of the precipitation of TiO_2 is governed by the acidity, the concentrations of Cl^- anions and the Ti complex in the solution. The elimination of chloride ligands from the titanium complexes lead to the formation of brookite or rutile crystallites. The growth of brookite or rutile on anatase was also studied by Penn and Banfield.[20] They proposed that the anatase (112) twin interfaces have one unit cell of brookite which has similar structure to that of rutile. Moreover, the twin interfaces consist of two slabs of octahedra arranged in a zigzag chain. In this manner, a number of such twin surfaces of anatase nanofibers can serve as seeds for the growth of both brookite and rutile crystallites. In addition, the defects formed at the interface between anatase and brookite must have acted as the potential sites for the nucleation of rutile phase.[21]

(3) Under the hydrothermal reaction, both brookite and rutile phases of TiO_2 can grow on the anatase nanofibers. However, when the ratio of Cl to Ti, in the solution is relatively high, the growth of brookite, and low, the growth of rutile is favored.[20] In the present work, at room temperature, the solution used had Cl : Ti ratio close to 140. In the autoclave, when the temperature of the solution gradually increased from room temperature to the pre-set reaction temperature, a fraction of the Cl^- in the solution must have escaped as HCl gas, and accumulated in the upper portion of the autoclave. This process led to a rapid decrease in the Cl : Ti ratio, and hence a decrease in the acidity of the solution as the temperature increased. As a result, at the beginning of the hydrothermal reaction, both the brookite and rutile seeds could have been nucleated at the twin planes of anatase surface layer. At relative low temperatures, the ratio Cl : Ti was high, and hence favored the growth of brookite as compared to that of rutile.[22] However, as the temperature increased, the Cl^- concentration in the solution decreased and hence favored the growth of rutile. Due to the tetragonal crystal structure of rutile, the nanorods in tetragonal shape grew outward the anatase nanofibers surface leading to the hierarchical nanostructures.

4. Conclusions

Novel homogenous TiO_2 hierarchical nanostructures, consisting of rutile rods on anatase nanofibers, have been successfully synthesized. The rough surface of the nanofibers and existence of rutile and brookite type structural units in anatase played important roles in the nucleation and growth of rutile nanorods. The Cl : Ti ratio in Ti–HCl solution decides the growth rate of brookite and rutile phases on the anatase nanofibers, and therefore, the size and the number density of the rutile nanorods could be controlled by adjusting the parameters of the hydrothermal reaction. The estimated band gap energies are very close to the respective literature values of the anatase and rutile phases of TiO_2. The surface area of the hierarchical nanostructures was close to 20.41 $m^2 g^{-1}$. The photocatalytic activity exhibited by the TiO_2 hierarchical nanostructures was superior to that of pure TiO_2 nanofibers. The experimental approach adopted in the present study can also be adopted in the synthesis of rutile rods on different anatase nanostructures such as nanotubes, nanopores, *etc.* The synthesised three dimensional TiO_2 nanostructures can be used for applications in different fields, such as sensor arrays, optoelectronic devices, solar cells, *etc.*

Acknowledgements

Financial support from the BK21 Project through the School of Advanced Materials Science & Engineering is gratefully acknowledged. The authors also appreciate the project and equipment support by the GRRC program through Gyeonggi Province (2010-B10) in Sungkyunkwan University and Basic Science Research Program though National Research Foundation of Korea (NRF) funded by Ministry of Education, Science and Technology (2010-0015035). One of the authors (Bhoraskar) is grateful to C. S. I. R., NewDelhi (India) for granting study leave on the post of Emeritus Scientist, and permission to work at SKKU, Suwon, South Korea.

References

1 D. J. Milliron, S. M. Hughes, Y. Cui, L. Manna, J. Li, L.-W. Wang and A. P. Alivisatos, *Nature*, 2004, **430**, 190; J. Y. Lao, J. G. Wen and Z. F. Ren, *Nano Lett.*, 2002, **2**, 1287; P. Gao and Z. L. Wang, *J. Phys. Chem. B*, 2002, **106**, 12653; K. A. Dick, K. Deppert, M. W. Larsson, T. Martensson, W. Seifert, L. R. Wallenberg and L. Samuelson, *Nat. Mater.*, 2004, **3**, 380; D. F. Zhang, L. D. Sun, C. J. Jia, Z. G. Yan, L. P. You and C. H. Yan, *J. Am. Chem. Soc.*, 2005, **127**, 13492.

2 X. Chen and S. S. Mao, *Chem. Rev.*, 2007, **107**, 2891; M. Gratzel, *Nature*, 2001, **414**, 338; A. Fujishima and K. Honda, *Nature*, 1972, **37**, 238; S. H. Lim, J. Luo, Z. Zhong, W. Ji and J. Lin, *Inorg. Chem.*, 2005, **44**, 4124; G. K. Mor, O. K. Varghese, M. Paulose and C. A. Grimes, *Sens. Lett.*, 2003, **1**, 42; S. Y. Choi, M. Mamak, N. Coombs, N. Chopra and G. A. Ozin, *Nano Lett.*, 2004, **4**, 1231; J. Joo, S. G. Kwon, T. Yu, M. Cho, J. Lee, J. Yoon and T. Hyeon, *J. Phys. Chem. B*, 2005, **109**, 15297.

3 D. Li and Y. Xia, *Nano Lett.*, 2003, **3**, 555.

4 E. Formo, E. Lee, D. Campbell and Y. Xia, *Nano Lett.*, 2008, **8**, 668; E. Formo, Z. M. Peng, E. Lee, X. M. Lu, H. Yang and Y. Xia, *J. Phys. Chem. C*, 2008, **112**, 9970; E. Formo, M. S. Yavuz, E. P. Lee, L. Lane and Y. Xia, *J. Mater. Chem.*, 2009, **19**, 3878; E. Formo, P. H. C. Camargo, B. Lim, M. Jiang and Y. Xia, *Chem. Phys. Lett.*, 2009, **476**, 56.

5 C. Wang, C. Shao, X. Zhang and Y. Liu, *Inorg. Chem.*, 2009, **48**, 7261; T. Cao, Y. Li, C. Wang, L. Wei, C. Shao and Y. Liu, *J. Sol-Gel Sci. Technol.*, 2010, **55**, 105; N. Wang, C. Sun, Y. Zhao, S. Zhou, P. Chen and L. Jiang, *J. Mater. Chem.*, 2008, **18**, 3909; R. Ostermann, D. Li, Y. D. Yin, J. T. McCann and Y. Xia, *Nano Lett.*, 2006, **6**, 1297.

6 M. Shang, W. Wang, L. Zhang, S. Sun, L. Wang and L. Zhou, *J. Phys. Chem. C*, 2009, **113**, 14727; Y. Dai, X. Lu, M. McKiernan, E. P. Lee, Y. Sun and Y. Xia, *J. Mater. Chem.*, 2010, **20**, 3157.

7 J. Y. Lao, J. G. Wen and Z. F. Ren, *Nano Lett.*, 2002, **2**, 1287.

8 B. Liu and E. S. Aydil, *J. Am. Chem. Soc.*, 2009, **131**, 3985; X. Feng, K. Shankar, O. K. Varghese, M. Paulose, T. J. Latempa and C. A. Grimes, *Nano Lett.*, 2008, **8**, 3781.

9 X. Zhang, S. Xu and G. Han, *Materials letter*, 2009, **63**, 1761.

10 A. Chaves, K. S. Katiyan and S. P. S. Porto, *Phys. Rev. B: Solid State*, 1974, **10**, 3522; T. Ohsaka, F. Izumi and Y. Fujiki, *J. Raman Spectrosc.*, 1978, **7**, 321; Y. H. Zhang, C. K. Chan, J. F. Porter and W. J. Guo, *J. Mater. Res.*, 2011, **13**, 2602; G. A. Tompsett, G. A. Bowmaker, R. P. Cooney, J. B. Metson, K. A. Rogers and J. M. Seakins, *J. Raman Spectrosc.*, 1995, **26**, 57.

11 D. Reyes-Coronado, G. Rodriguez-Gattorno, M. E. Espinosa-Pesqueira, C. Cab, R. de Coss and G. Oskam, *Nanotechnology*, 2008, **19**, 145605.

12 P. Kubelka, *J. Opt. Soc. Am.*, 1948, **38**, 448; L. Yang and B. Kruse, *J. Opt. Soc. Am. A*, 2004, **21**, 1933; L. Yang and S. J. Miklavcic, *J. Opt. Soc. Am. A*, 2005, **22**, 1866.

13 J. Tauc, R. Grigorovici and A. Vancu, *Phys. Status Solidi B*, 1966, **15**, 627; N. Serpone, D. Lawless and R. Khairutdinovt, *J. Phys. Chem.*, 1995, **99**, 16646.

14 H. Zhang and J. F. Banfield, *J. Mater. Chem.*, 1998, **8**, 2073.
15 E. Bae, N. Murakami and T. Ohno, *J. Mol. Catal. A: Chem.*, 2009, **300**, 72.
16 J. Ovenstone and K. Yanagisawa, *Chem. Mater.*, 1999, **11**, 2770.
17 T. Kawahara, Y. Konishi, H. Tada, N. Tohge, J. Nishii and S. Ito, *Angew. Chem. Int. Ed.*, 2002, **41**, 2811; T. Kawahara, T. Ozawa, M. Iwasaki, H. Tada and S. Ito, *Journal of Colloid and Interface Science*, 2003, **267**, 377; L. Shi and D. Weng, *Journal of Environmental Sciences*, 2008, **20**, 1263; T. Ohno, K. Tokieda, S. Higashida and M. Matsumura, *Applied Catalysis A: General*, 2003, **244**, 383.
18 A. Testino, I. R. Bellobono, V. Buscaglia, C. Canevali, M. D'Arienzo, S. Polizzi, R. Scotti and F. Morazzoni, *J. Am. Chem. Soc.*, 2007, **129**, 3564.
19 X. Meng, J. H. Lee, M. Park, S. M. Yu, D. Shin, C. Yang, V. Bhoraskar and J. Yoo, *CrystEngComm*, 2011, DOI: 10.1039/C0CE00643B.
20 R. L. Penn and J. F. Banfield, *American Mineralogist*, 1998, **83**, 1077; R. L. Penn and J. F. Banfield, *American Mineralogist*, 1999, **84**, 871.
21 Y. Hu, H. L. Tsai and C. L. Huang, *Material Science and Engineering A*, 2003, **344**, 209.
22 A. Pottier, C. Chaneac, E. Tronc, L. Mazerolles and J. P. Jolivet, *J. Mater. Chem.*, 2001, **11**, 1116.